Water Vapor Tracers as Diagnostics of the Regional Hydrologic Cycle

MICHAEL G. BOSILOVICH AND SIEGFRIED D. SCHUBERT

Data Assimilation Office, NASA Goddard Space Flight Center, Greenbelt, Maryland

(Manuscript received 11 April 2001, in final form 2 November 2001)

ABSTRACT

Numerous studies suggest that local feedback of surface evaporation on precipitation, known recycling, is a significant source of water for precipitation. Quantitative results on the exact amount of recycling have been difficult to obtain in view of the inherent limitations of diagnostic recycling calculations. The current study describes a calculation of the amount of local and remote geographic sources of surface evaporation for precipitation, based on the implementation of three-dimensional constituent tracers of regional water vapor sources [termed ''water vapor tracers'' (WVTs)] in a general circulation model. The major limitation on the accuracy of the recycling estimates is the veracity of the numerically simulated hydrological cycle, though it is noted that this approach also can be implemented within the context of a data assimilation system. In the WVT approach, each tracer is associated with an evaporative source region for a prognostic three-dimensional variable that represents a partial amount of the total atmospheric water vapor. The physical processes that act on a WVT are determined in proportion to those that act on the model's prognostic water vapor. In this way, the local and remote sources of water for precipitation can be predicted within the model simulation and validated against the model's prognostic water vapor. As a demonstration of the method, the regional hydrologic cycles for North America and India are evaluated for six summers (June, July, and August) of model simulation. More than 50% of the precipitation in the midwestern United States came from continental regional sources, and the local source was the largest of the regional tracers (14%). The Gulf of Mexico and Atlantic regions contributed 18% of the water for midwestern precipitation, but further analysis suggests that the greater region of the tropical Atlantic Ocean may also contribute significantly. In most North American continental regions, the local source of precipitation is correlated with total precipitation. There is a general positive correlation between local evaporation and local precipitation, but it can be weaker because large evaporation can occur when precipitation is inhibited. In India, the local source of precipitation is a small percentage of the precipitation, owing to the dominance of the atmospheric transport of oceanic water. The southern Indian Ocean provides a key source of water for both the Indian continent and the Sahelian region.

1. Introduction

Interannual variability of hydrometeorology (e.g., drought and flood) can have a devastating impact on a region's society and economy. Improved understanding of the variability and extremes of the hydroclimate through diagnostic study should benefit long-term forecasting, disaster preparedness, and allocation of resources (e.g., energy and water conservation). The processes that initiate and maintain drought and flood have been a significant concern, especially considering that global change may exacerbate the intensity of these hydrologic anomalies. Therefore, it is important to diagnose and understand the complete hydrologic cycle. Many questions remain regarding the geographic source of water in precipitation. For example, how much precipitation originates from local evaporation in comparison with water that has been transported for some distance?

Koster et al. (1986) introduced passive tracers in a GCM that have a source equal to the evaporation from a prescribed continent or ocean and used model sources and sinks of water (condensation, reevaporation, convection, and advection) to compute tendencies of the passive tracer. In this paper, we call such passive tracers ''water vapor tracers'' (WVTs). In this way, water was ''tagged'' at its surface source and followed through atmospheric processes until it precipitated from the atmosphere. The results differentiated between continental and oceanic sources of water vapor that contribute to precipitation. The simulations were performed with coarse resolution ($8^\circ \times 10^\circ$, nine layers), and the results were for 1-month periods. The amount of water that evaporates and then precipitates within the same region [precipitation recycling, as defined by Eltahir and Bras (1996)] was not addressed.

Joussaume et al. (1986) describe a similar method of diagnosing the origin of precipitation by predicting the three-dimensional transport of water that evaporated at

Corresponding author address: Michael G. Bosilovich, Data Assimilation Office, NASA Goddard Space Flight Center, Code 910.3, Greenbelt, MD 20771.
E-mail: mikeb@dao.gsfc.nasa.gov

the surface of a distinct region as a passive constituent of the atmosphere. The formulation of sources and sinks of WVTs is discussed in detail, including evaporation, condensation, re-evaporation, diffusion, advection, and convection. The WVT is predicted forward in time from its source by surface evapotranspiration until it precipitates back to the surface, including all the model-simulated processes that act on the model's prognostic water vapor. It was noted that positive definite advection is required for these simulations, and a forward advection scheme was used. This effort demonstrated the range of influence of the oceans on continental precipitation but did not evaluate local precipitation recycling or the interannual variability of the source regions. Nonetheless, these experiments described a methodology that should also provide significant diagnostic information when studying regional hydrologic cycles (such as those associated with the North American and Indian monsoons). Recently, Numagati (1999) used this methodology to study the Eurasian regional sources of precipitation.

To diagnose the sources of North American precipitation, Dirmeyer and Brubaker (1999) used a diagnostic method of analyzing quasi-isentropic back trajectories of water vapor. The method uses 6-hourly estimates of National Centers for Environmental Prediction (NCEP) reanalysis wind, water vapor, and evaporation and hourly precipitation observations to determine the regional sources of precipitation. An advantage to this method is that the kinds of data used by the system are flexible (model, analysis, or observation data can be inserted). Another advantage is that the computations are less intensive than performing multiyear GCM simulations or reanalyses. However, the initialization of the quasi-isentropic tracers depends on a statistical distribution of the precipitation, and the movement and extraction of water do not depend on the physical tendencies included in the reanalysis. The back-trajectory method does provide estimates of precipitation recycling.

Bulk diagnostic recycling methods evaluate monthly mean precipitation, evaporation, and moisture transport to compute precipitation recycling (Brubaker et al. 1993; Eltahir and Bras 1994). These methods use vertically integrated water vapor transport and assume that the local source of water is mixed well with all other sources of water in the whole vertical column. Studies by Trenberth (1999) and Bosilovich and Schubert (2001) used these methods to evaluate the spatial and interannual variability of the local source of water (precipitation recycling). These methods are computationally efficient, but they may be hindered by simplifications—most notable, a lack of short-timescale correlations between the hydrological parameters (in particular, the diurnal and synoptic timescales). These models provide solely the local source of water and do not include the remote sources of water for a region.

There are many uses for a quantitative diagnostic that can distinguish the local and remote sources of water that precipitates. For example, Barnston and Schikedanz (1984) found that irrigation could enhance precipitating events (by studying observations of precipitation and irrigation trends) but only when a mechanism to trigger the precipitation was present (e.g., a thunderstorm or squall line). Huang et al. (1996) used a simple model for soil moisture to determine evaporation from monthly mean temperature and precipitation. The results show that evaporation variability is much smaller than precipitation variability, suggesting that the local source of water is less important to precipitation anomalies. Klein and Bloom (1989) studied the statistical relationship between precipitation events and the 700-mb atmospheric circulation in order to improve prediction of seasonal precipitation. From these relationships, the direction of dominant low-level flow contributing to precipitation could be determined and the remote source of water could be inferred. These studies lack a quantified budget of the local and remote sources of water in the regional hydrological processes.

This paper describes the implementation and validation of regional water vapor tracers in a GCM following the methodology used by Koster et al. (1986) and Joussaume et al. (1986). Their application was designed to address global issues. We will evaluate and validate the methodology for use in regional studies. Section 2 describes the model structure, experimental design, and tracer formulation. In section 3, the model water, precipitation, and WVTs are validated and the local and remote sources of water for precipitation over India and North America are examined. The precipitation recycling from the WVTs is compared with bulk diagnostic recycling methods.

2. Model and methodology

a. GEOS GCM

The base model used in this study is version 3 of the Goddard Earth Observing System (GEOS-3) GCM (Suarez and Takacs 1995). The moisture and tracer advection is calculated by a positive definite semi-Lagrangian method (Lin and Rood 1996) on the Arakawa C grid, and the temperature advection is computed by a fourth-order scheme. The model physics includes relaxed Arakawa–Schubert (RAS) convection (Moorthi and Suarez 1992) with rain evaporation (Sud and Molod 1988), parameterization of shortwave (Harshvardhan et al. 1987) and longwave (Chou 1984) radiation, and a level-2.5 boundary layer turbulence closure scheme (Helfand and Labraga 1988). Recent improvements to the GEOS GCM include the addition of the Mosaic land surface model (Koster and Suarez 1992) and the incorporation of subgrid moist processes in turbulent diffusion (Helfand et al. 1999). The Mosaic land surface model includes prognostic soil water, temperature, and snow and mosaic heterogeneity. The GEOS-3 GCM is a component of the GEOS-3 data assimilation system

that is being used to support the Earth Observing System *Terra* and Aqua missions at the National Aeronautics and Space Administration (NASA).

b. Water vapor tracers

This section describes the implementation of the WVT diagnostics into the GCM. The prognostic equation for water vapor is

$$\frac{\partial q}{\partial t} = -\nabla_3 \cdot (qV) + \left.\frac{\partial q}{\partial t}\right|_{\text{turb}} + \left.\frac{\partial q}{\partial t}\right|_{\text{cond}} + \left.\frac{\partial q}{\partial t}\right|_{\text{revp}} + \left.\frac{\partial q}{\partial t}\right|_{\text{RAS}}. \quad (1)$$

At any one point in the atmosphere, the physical tendencies that act on the water vapor are turbulence (turb), which includes surface evaporation, and the moist tendencies occurring because of large-scale precipitation and RAS convection parameterizations, which include condensation (cond), rain evaporation (revp), and redistribution by convection (RAS). The transport of water is critical to this experiment. Joussaume et al. (1986) suggest that a positive definite advection scheme is required for tracer transport, and they employed a forward scheme. In the current study, the model calculates moisture and tracer advection by a positive definite semi-Lagrangian scheme developed by Lin and Rood (1996). Tests with a fourth-order advection scheme demonstrated that significant corrections are needed for filling of negative values.

In the framework of a GCM, constituents of the atmosphere can be incorporated easily into the dynamical and physical framework, especially if these constituents are passive (i.e., do not affect or interact with the fundamental state variables of temperature, moisture, and wind). In general, passive constituents are implemented in the GCM as three-dimensional prognostic variables and can be referred to as tracers. In our case, we would like to compute for precipitation in one region the contributions of water that originated locally and in remote evaporation regions. To accomplish this goal, three-dimensional passive constituent tracers will use surface evaporation from a prescribed region as their origin. These constituents are predicted forward in time (at the model's time step), parallel to the model's prognostic water vapor variable. The same physical processes that act on water vapor also act on the passive constituents, including precipitation. Therefore, given a finite area of evaporation, we can determine the contribution of that region's surface evaporation to water vapor and precipitation at any point on the globe. In this implementation, the passive constituent tracers of regional water vapor are the WVTs.

If each model grid point's evaporation contributes to one WVT, then the sum of all WVTs will equal the prognostic water vapor ($\Delta q' = 0$), where

$$\Delta q'(x, y, \sigma, t) = q(x, y, \sigma, t) - \left[\sum_{n}^{N_T} q_{Tn}(x, y, \sigma, t) + q_{TC}(x, y, \sigma, t)\right]. \quad (2)$$

Here, q is the water vapor, q_{Tn} is defined as any regional WVT, N_T is the total number of regional tracers, and q_{TC} is introduced as the complement tracer, which incorporates all surface evaporation sources not included in a regional tracer. The space and time dimensions are x, y, σ, and t for longitudinal, latitudinal, vertical, and temporal dimensions, respectively. For the experiments presented here, regional tracers are initially set to 0, and the complement tracer is initially set equal to water vapor at every point [$q_{TC}(x, y, \sigma, t) = q(x, y, \sigma, t)$]. As the model integrates forward in time, the regional tracers will receive their region's evaporative source but will take some time to spin up. In general, the spinup takes less than 2 weeks of simulation, but a month of spinup time is provided to each simulation. A separate experiment shows that the *e*-folding time of water to be precipitated is 8.5 days, and after 30 days less than 3% of the initial water remains in the atmosphere. Because the WVTs are passive and separate from the prognostic water vapor, this also provides a fundamental validation for the development of the model code, where $\Delta q'$ ideally should always be 0.

The prognostic equation for any one tracer is

$$\frac{\partial q_T}{\partial t} = -\nabla_3 \cdot (q_T V) + \left.\frac{\partial q_T}{\partial t}\right|_{\text{turb}} + (E_{\text{surf}})_T + f_C \left.\frac{\partial q}{\partial t}\right|_{\text{cond}} + f_R \left.\frac{\partial q}{\partial t}\right|_{\text{revp}} + f_{\text{RAS}} \left.\frac{\partial q}{\partial t}\right|_{\text{RAS}}. \quad (3)$$

Turbulent tendency of the WVTs occurs whenever tracer water is present, but positive surface evaporation may only be occurring in a tracer's finite source region [$(E_{\text{surf}})_T$]. Further, the evaporative sink of tracers (owing to dew formation) is considered to be proportional to the ratio of tracer water and total water vapor near the surface. Tracer water is assumed to be mixed well with the total water vapor at each three-dimensional grid point. Therefore, the physical tendencies of tracer water by precipitation processes are computed proportional to the tendencies of total water vapor. Note that condensation and rain evaporation terms include both large-scale and convective tendencies, and the RAS subscript indicates the convection (or redistribution of water) by the relaxed Arakawa–Schubert convection scheme. The proportionality relationships for condensation f_C, rain evaporation f_R, and RAS convective redistribution f_{RAS} are given by

$$f_C(L) = \frac{q_T(L)}{q(L)},$$

$$f_R(L) = \frac{\int_1^{L-1} \left(\left.\frac{\partial q_T}{\partial t}\right|_{\text{cond}} + \left.\frac{\partial q_T}{\partial t}\right|_{\text{revp}} \right) d\sigma}{\int_1^{L-1} \left(\left.\frac{\partial q}{\partial t}\right|_{\text{cond}} + \left.\frac{\partial q}{\partial t}\right|_{\text{revp}} \right) d\sigma}, \quad \text{and}$$

$$f_{\text{RAS}}(L) = \begin{cases} \dfrac{q_T(L)}{q(L)} & \left.\dfrac{\partial q}{\partial t}\right|_{\text{RAS}} < 0 \\ \dfrac{\int_{\text{LM}}^{L+1} \left.\dfrac{\partial q_T}{\partial t}\right|_{\text{RAS}} d\sigma}{\int_{\text{LM}}^{L+1} \left.\dfrac{\partial q}{\partial t}\right|_{\text{RAS}} d\sigma} & \left.\dfrac{\partial q}{\partial t}\right|_{\text{RAS}} > 0, \end{cases} \tag{4}$$

where L is a given model level, LM is the lowest model level closest to the surface, and $L = 1$ is the top of the model (0.1 hPa). Integrations are done on the sigma vertical coordinate. To close this set of equations, some conditions must be applied. If the proportionality requires the use of the tracer water and specific humidity, the previous time-step data are used in the calculation. If tendencies are required, the current time-step specific humidity tendencies are used. The following boundary conditions are applied to solve the integrations:

$$\left.\frac{\partial q}{\partial t}\right|_{\text{RAS}} \le 0 \qquad L = \text{LM}, \quad \text{and}$$

$$\left.\frac{\partial q}{\partial t}\right|_{\text{cond}}, \qquad \left.\frac{\partial q}{\partial t}\right|_{\text{revp}} = 0 \qquad L = 1. \tag{5}$$

That is, the convective mass flux takes away water from the near-surface layers, and the model does not produce condensation and rain evaporation at the top of the model.

The proportionality rules can be summarized as follows: sinks of tracer water consider the ratio of tracer water to total water vapor at a level (e.g., condensation of water), and sources of tracer water consider the ratio of vertically integrated stores of tracer water and water vapor during vertical processes at a given time (e.g., rain evaporation).

It should be reiterated that the WVTs are being computed at the model time step as prognostic equations. The WVTs are predicted from model tendencies for water vapor but do not affect the model's state variables. The prognostic water vapor variable is used in the model precipitation, convection, and radiation processes. The precipitation of any WVT at any time or grid point is computed by

$$P_T = -\frac{p_s}{g} \int_1^{\text{LM}} \left(\left.\frac{\partial q_T}{\partial t}\right|_{\text{cond}} + \left.\frac{\partial q_T}{\partial t}\right|_{\text{revp}} \right) d\sigma, \tag{6}$$

where p_s and g are the surface pressure and gravitational acceleration, respectively. The subsequent analysis of the model data will rely on, for the most part, monthly averages. To compute the recycling ratio, we will use monthly total and local precipitation area averaged over the source region for each month. This approach will provide a time series that can be used to determine the seasonal mean and statistical relationships.

c. Experimental design

The above algorithm for the WVTs was implemented in the GEOS-3 GCM. For the experiments described here, the model was run at a horizontal resolution of 2° × 2.5°, and 48 vertical levels. Six summer-season simulations were performed, including WVTs for the North American and Indian regions. The seasonal simulations are initialized on 1 May (for 1990–95), from an existing 10-yr model simulation and are run through the end of August. Sea surface temperature and sea ice are prescribed from monthly observations provided by NCEP (Reynolds and Smith 1994). Thirteen regional tracers are defined, with 14th tracer defined as the complement of the 13 regions (includes surface evaporation from the rest of the globe). Note that because each grid point's surface evaporation is included in only one WVT, the sum of all WVTs [as in Eq. (2)] should ideally be equal to the GCM's prognostic water vapor. Differences that occur later in the simulation can be used to validate the tracer formulation.

Note that we use only 13 regional tracers, but that 19 regions are identified in Fig. 1 between India and North America. Previous studies showed that the Indian Ocean does not have much influence on North America as a source of water (Joussaume et al. 1986; Druyan and Koster 1989). The regional tracers in this experiment cover smaller areas than in previous studies. Because it is unlikely that the two distant regions' tracers would interfere, we include two geographic regions as a source for a single water vapor tracer. For example, this experiment uses the same three-dimensional tracer to account for both the southwestern United States (SW) and the Indian continental (IN) evaporation. Furthermore, this will improve the efficiency of the model simulation regarding computing power. The risk, of course, is that IN evaporation could be misdiagnosed as an SW source in North America. The purpose here is to test the viability of multiple regions in a single WVT as a way to optimize computing resources.

3. Results

In this section, we present the results of the numerical simulations. First, the mean summer [June, July, and August (JJA)] total precipitable water (TPW) and precipitation are compared with observations. The WVT methodology is validated against the model-simulated water variables (TPW and precipitation). Local and re-

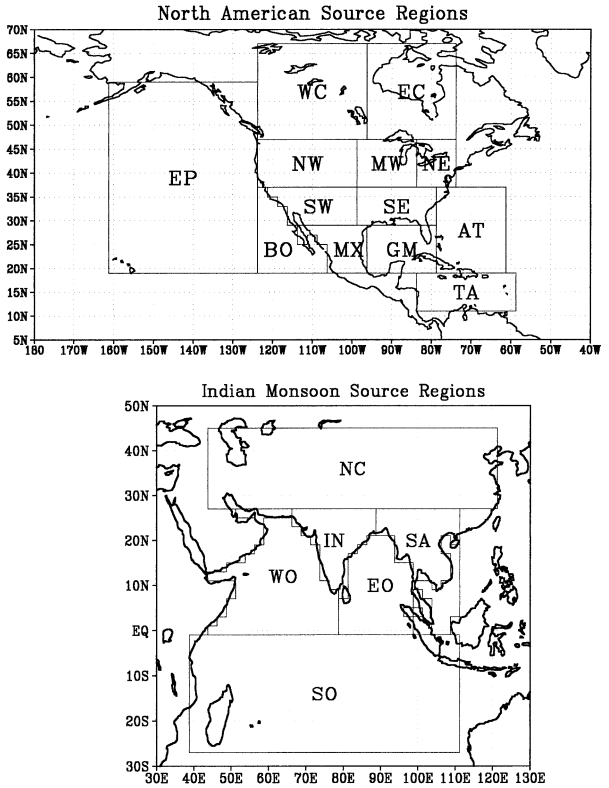

FIG. 1. Sources of surface evaporation for regional tracers; MW: Midwest, SE: Southeast, SW: Southwest, NW: Northwest, WC: west Canada, EC: east Canada, NE: Northeast, AT: Atlantic, TA: tropical Atlantic, GM: Gulf of Mexico, MX: Mexico, BO: Baja oceanic, EP: east Pacific, IN: India, EO: east oceanic, SO: south oceanic, WO: west oceanic, SA: Southeast Asia, and NC: north continental.

mote sources of water for precipitation in the North American and Indian regions are presented, and bulk diagnostic methods of computing precipitation recycling are compared with WVT recycling.

a. Simulation of water vapor and precipitation

Figure 2 compares the modeled precipitation and TPW over North America with observations. In comparison with the observed TPW (Simpson et al. 2001), GEOS is wetter in the Gulf of Mexico but drier in the western United States. In general, the simulation produces too much precipitation [as compared with Xie and Arkin (1997) observations] in the central United States, the Gulf of Mexico, continental Mexico, and the Atlantic Ocean. A swath of large precipitation extends from the central United States to Newfoundland. In the Indian region (Fig. 3), the model-simulated TPW is comparable to observations (with the only notable exception being that the deserts are drier). The pattern of precipitation matches with the observations, but the areas of strong convection show too much simulated precipitation. At the global scale, the model's TPW and precipitation are in line with the observations (Fig. 4). Although some differences with the observations are apparent, the simulated fields are generally realistic.

b. Validation of WVTs

The model predicts global water vapor as described by Eq. (1). This is entirely separate from the prediction of the WVTs. By design, each grid point's surface evaporation provides a source for only one WVT (one of the 13 regional tracers or the complement tracer). Therefore, the sum of the regional WVTs and the complement WVT ideally should be equal to the model's prognostic water vapor [$\Delta q' = 0$ in Eq. (2)], and we shall use this fact to determine the uncertainty of the WVT methodology.

Figure 5 compares the model's simulated TPW and precipitation to both the sum of all tracer water and the sum of all tracer precipitation from one simulation that was extended several months beyond JJA. The differences are globally averaged every three hours. The standard deviation of the global differences is also included. Regional tracers are initialized at 0, and the complement tracer is equal to the specific humidity, so that the sum of the tracers is initialized to the model's total water. In the first few weeks, the sum of tracer water spins up to a value that is slightly smaller than the model's water (by -0.05 cm, or $\sim$2%). During the spinup period, there is an overestimate of precipitation by the tracers. The excessive tracer precipitation reduced the total tracer water to a stable point at which the tracer precipitation matches the modeled precipitation. So, although there is little bias in the global precipitation, the standard deviation of the difference is about 0.2 mm day^{-1} ($\sim$5%). Figure 6 shows the zonal mean difference of JJA (all six years) water vapor and total WVTs. The largest difference is about -0.25 g kg^{-1} near a relative minimum of zonal precipitation (10°–20°S). In general, the differences are small in the lower troposphere, below the convective cloud base, and are larger within the cloud.

The error in the WVTs is small but is larger than truncation error. After a review of the code, the differences were found to be primarily resulting from calls to the RAS routine and the WVT routine at different time steps (the WVTs were being updated every time step, RAS less frequently). A secondary error was introduced due to subgrid terms in the semi-Lagrangian advection that react to the different horizontal gradients of tracers and specific humidity. Fixing the code reduced the errors to computer truncation but did not appreciably change the simulation of WVTs in a test case (only one season). The only similar data presented in the refereed literature are by Koster et al. (1986). However, only monthly differences are presented, and their regional tracer precipitation shows some small differences when compared with the model's simulated precipitation (near $\pm$1%). Table 1 shows all the sources of water for North American land regions. The last column of Table 1

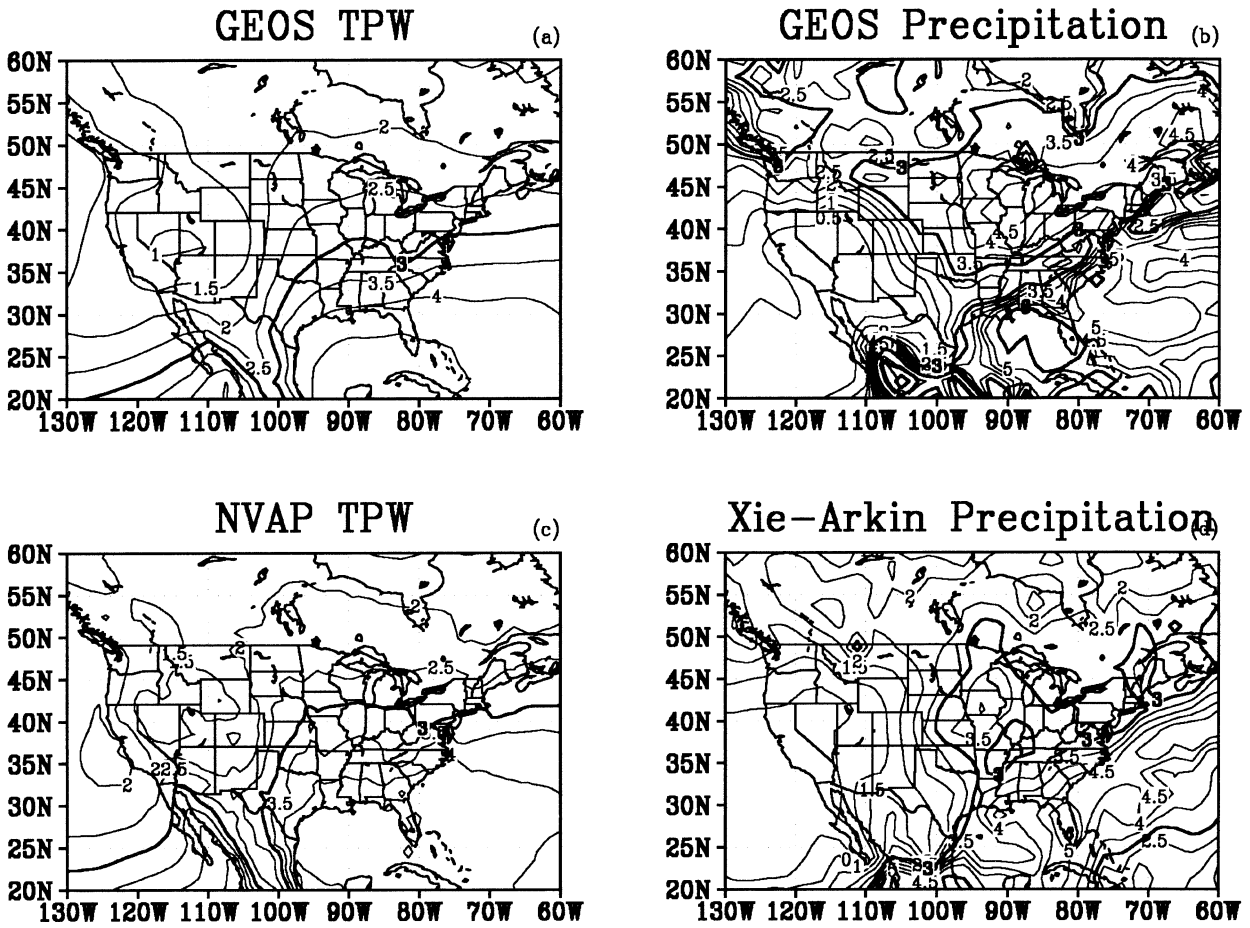

FIG. 2. Comparison of GEOS with observations of TPW for 1990–94 (cm) and precipitation for 1990–95 (mm day^{-1}) for the JJA average over the North American region (contour intervals of 0.5, 1.0, 1.5, 2.0, 2.5, 3.0, 3.5, 4.0, 4.5, 5.0, 6.0, 8.0, 12.0, 16.0, and 20.0; the contours divisible by 3 are boldface). TPW observations are from NASA's Water Vapor Project (NVAP; Simpson et al. 2001) and precipitation observations are from Xie and Arkin (1997; JJA 1990–95).

indicates that we obtain small differences for seasonal means near those of Koster et al. (1986). The small errors likely do not affect the overall results in this study.

c. North American local and remote sources of water

In this section, North American (see Fig. 1) JJA hydrological behavior is investigated using the WVTs. This region is influenced by a blend of large-scale forcing of the moisture transport (Bermuda high and Rocky Mountains), the Great Plains low-level jet, and local convective processes (Helfand and Schubert 1995; Higgins et al. 1997; Bosilovich and Sun 1999a). The source regions defined in Fig. 1 were designed to isolate significant contributors to precipitation in the central United States.

Figure 7 shows the total precipitation and the percentage of each regional WVT's precipitation over North America. This figure demonstrates the extent of the contribution of each region to the North American precipitation. Southerly flow that dominates the central United States prevents the Midwest (MW) region from influencing the Southeast (SE), and likewise carries SE and SW water into MW. The Pacific Northwest (NW) region influences much of North America because of the mean zonal flow. The Atlantic (AT) region affects the United States east of the Mississippi River and produces much precipitation from the Gulf of Mexico and Gulf Stream. The Gulf of Mexico (GM) strongly affects the SE and MW regions and even influences the east coast of Canada (EC). A certain amount of water reaches the central United States from Mexico (MX), but the Baja Oceanic (BO) region does not contribute to precipitation north of MX or southwest of the ITCZ. Note that the model tends to produce a high-bias swath of precipitation from the central United States to Newfoundland (as much as 1 mm day^{-1} in Fig. 2b), but there is not a clear regional, continental, or oceanic source tied to the high bias. It is possible that either the model is producing too much surface evaporation everywhere or the precipitation mechanisms are leading to the bias. It is beyond the scope of this study to pursue sensitivity

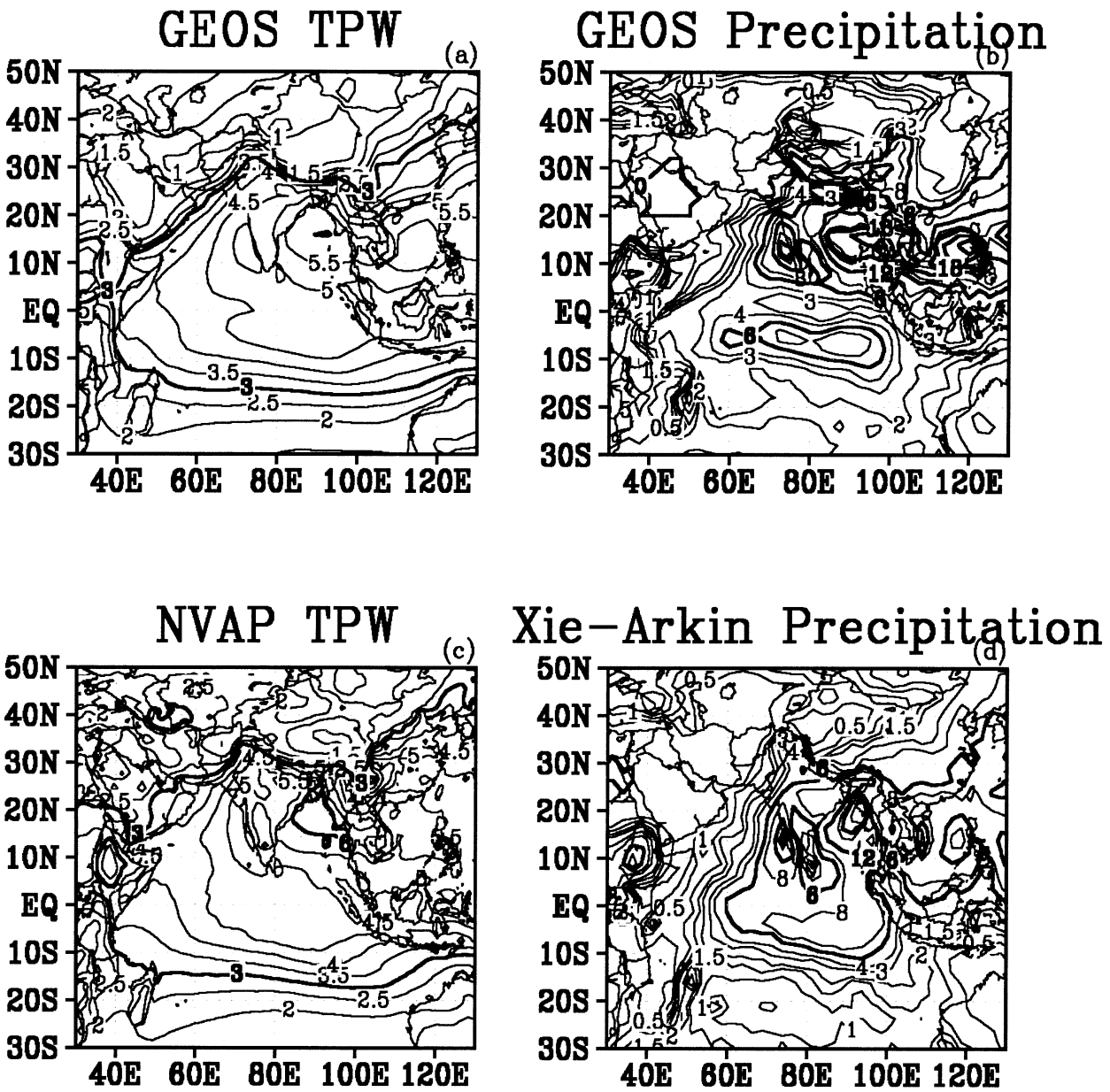

FIG. 3. As in Fig. 2, but for the Indian Ocean region (contour intervals of 0.5, 1.0, 1.5, 2.0, 3.0, 4.0, 6.0, 8.0, 12.0, 16.0, and 20.0; TPW contours divisible by 3 cm and precipitation contours divisible by 6 mm day^{-1} are both boldface).

and model development; rather, this result points to a potential use of the WVT methodology to diagnose model deficiencies.

Figure 8 shows the mean JJA moisture transport and evaporation and helps to explain some of the features in Fig. 7. Strong evaporation and the easterly flow across the tropical Atlantic Ocean provide the water for the MW and SE regions. Moderate evaporation that occurs in the east SW region is transported by the southerly flow associated with the low-level jet into the MW region. The long fetch of the NW region, moderate evaporation toward eastern NW, and zonal flow carry moisture toward the MW region. The eastern Pacific (EP) region shows strong northerly flow along NW that prevents much moisture from entering the United States. The vertex of this northerly flow and the southerly flow of the Bermuda high occurs between the BO and MX regions. In the mean sense, little water from BO can cross this vertex and move to the central United States. Rather, as Fig. 7 shows, the BO water is carried by the easterly flow to the ITCZ (but some does precipitate in western Mexico). However, moisture evaporated in east MX is far enough from the vertex to be transported by the southerly flow into the United States. The general

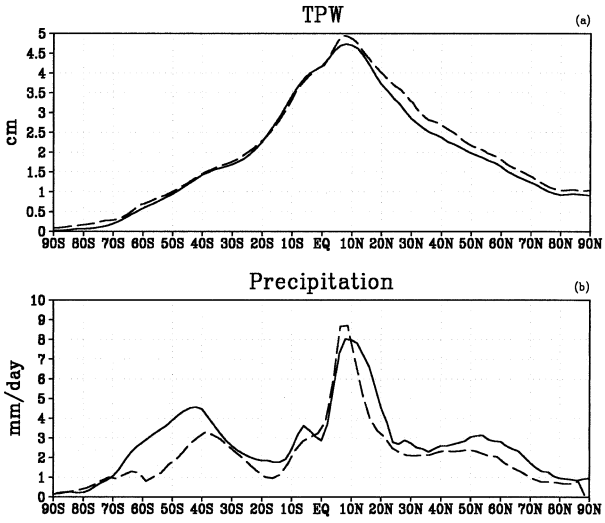

FIG. 4. (a) Zonal mean JJA 1990–94 TPW (cm) for GEOS (solid) and NVAP (dashed). (b) Zonal mean JJA 1990–95 precipitation (mm day^{-1}) for GEOS (solid) and Xie and Arkin (1997) (dashed).

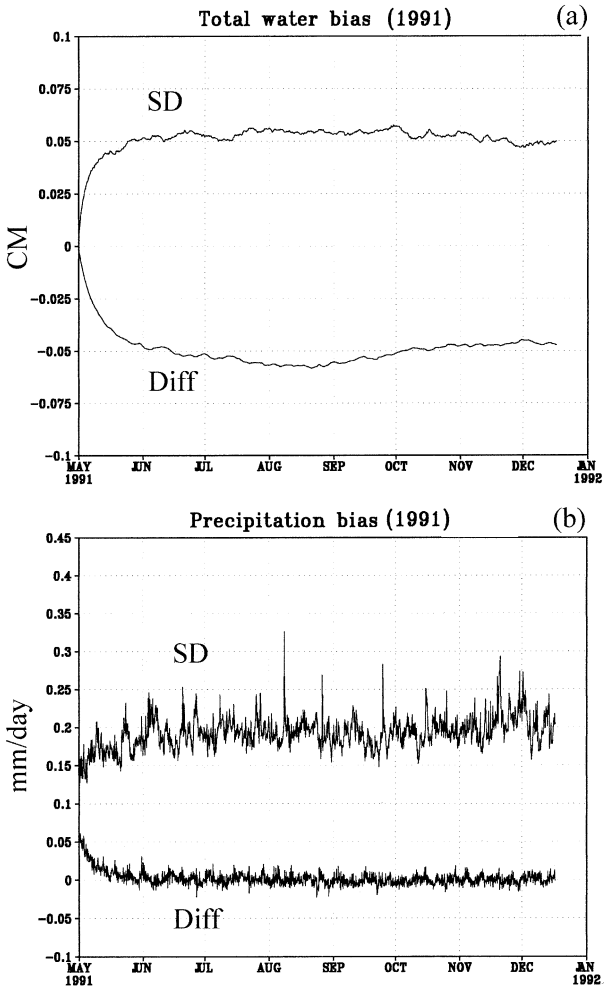

FIG. 5. Time series of global mean differences (Diff) and standard deviations (SD) of the global difference map of the model minus sum of all tracers for (a) TPW and (b) precipitation. Data points are 3-hourly. Of the six, this is one representative year that was continued until mid-December.

pattern of the moisture transport (including this southwestern vertex of the flow) is comparable to that presented by Peixoto and Oort (1992, their Fig. 12.17c). We can use the moisture transport map to discuss the mean circulation of the atmospheric branch of the hydrologic cycle, and WVT diagnostics quantify the sources and sinks of the regional hydrological processes.

Table 1 shows the percentage of precipitation that occurs in each of the North American land regions from all the WVTs. The time averages are computed from the area average of monthly mean WVT and total precipitation. Despite being a relatively small region [as compared with the Brubaker et al. (1993) central U.S. region], MW provides the largest source of water to the MW region (14.3%), and the sum of AT, tropical Atlantic (TA), and GM is about 18%. Regional continental sources make up more than one-half of the total water that precipitates in the MW region. Continental evaporation is an important source of water for the Midwest, and the local source is only a part of that. This result implies that the ability of the model to simulate precipitation in this region is strongly influenced by the land parameterization, especially the formulation of evapotranspiration.

The SE region is dominated by the oceanic sources, especially GM. However, recycling does account for 13% of the precipitation, and 34% of the sources are unaccounted for by our regional tracers. Some of the unaccounted water is likely related to the tropical Atlantic Ocean closer to Africa (to be examined later in the analysis). The SW sources are diverse, with contributions from most of the nearby regions, though the magnitude of SW total precipitation and recycled precipitation are small (Table 2). The NW region exhibits a large local source of precipitation, much larger than the contribution of water from EP. A long fetch and evaporation that exceeds precipitation help to explain the importance of the local water source to the NW region during JJA. The MW and SE regions contribute to the NE precipitation because of their proximity, but GM and AT are also very important components. The MX region has some of the largest total and recycled precipitation of the regions studied (Table 2). The lack of a tropical Pacific Ocean source in the regional tracers limits our ability to analyze the MX sources of water.

Figure 9 shows the mean seasonal variation of the sources of water for the MW, SE, SW, and MX regions. In the MW region, the sources from GM and TA show an increase during the summer season. The SE source for MW does not show a systematic variation within JJA, but the interannual variability (as denoted by the standard deviation bars) is larger than that of the MW region. Within the SE region, the sources of water from GM and AT (and the local source) increase from June

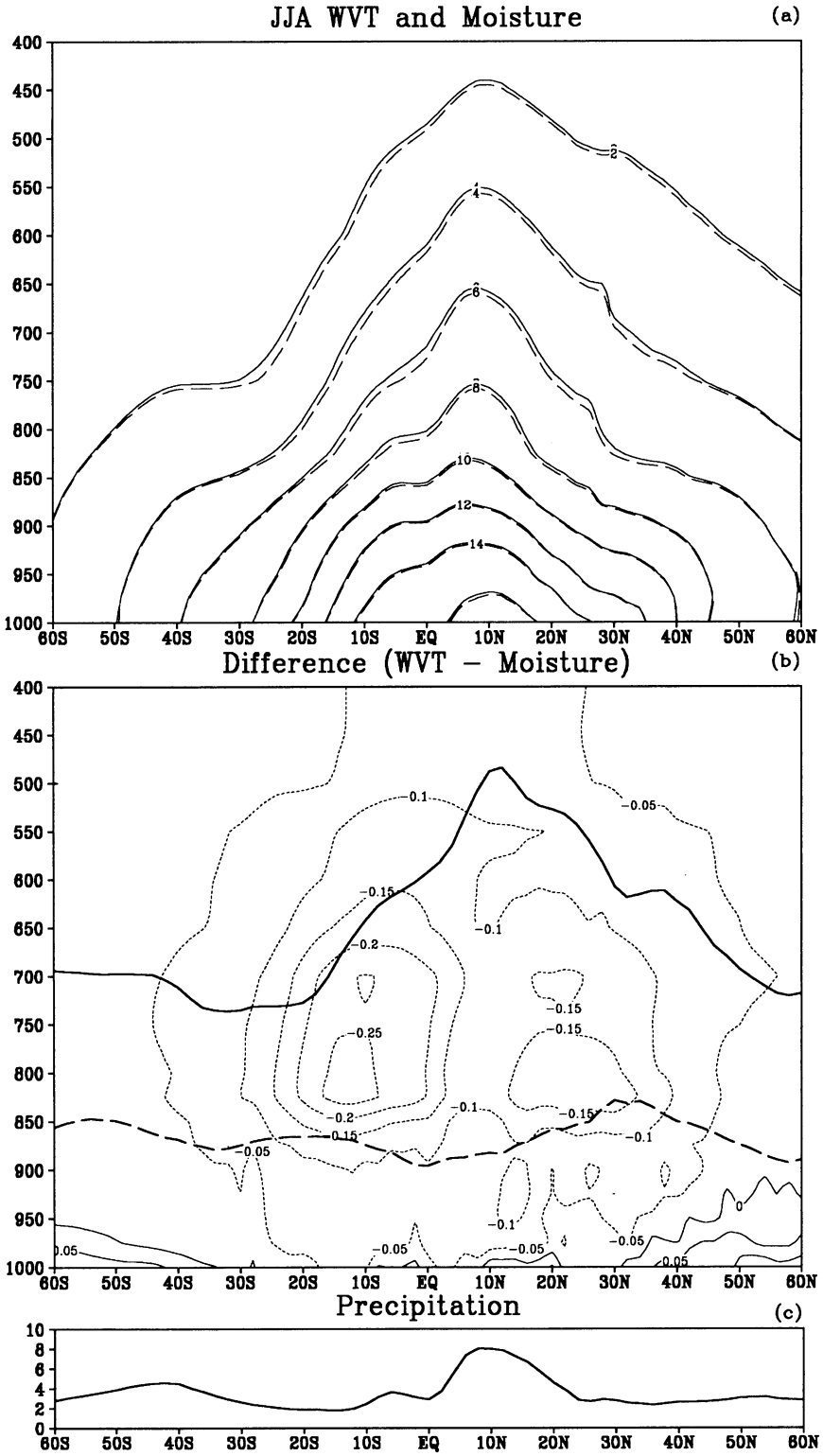

FIG. 6. Zonal average of the (a) JJA mean specific humidity (solid) and total WVTs (dashed), (b) difference of total WVTs and specific humidity (the solid line indicates cloud top and the dashed line indicates the relaxed Arakawa–Schubert cloud base), and (c) JJA precipitation. The data are time averaged for all six JJAs. Units are grams per kilogram for specific humidity, water vapor tracer, and their difference and millimeters per day for precipitation.

TABLE 1. Percentage of total precipitation in destination (1st column) occurring from evaporation in the source regions, averaged for JJA. Boldface values highlight the local source of precipitation (recycling). The difference of the sum from 100% is associated with the difference of the tracers and modeled precipitation. ''Comp'' is the complement WVT and consists of the rest of the globe not included in regional WVTs.

	Source														
Destination	MW	SE	SW	NW	WC	EC	NE	AT	TA	GM	MX	BO	EP	Comp	Sum
Midwest (MW)	**14.3**	12.6	4.7	10.1	4.8	2.0	1.2	4.5	3.3	9.9	4.0	1.6	4.3	23.1	100.3
Southeast (SE)	1.4	**12.7**	1.8	2.0	1.0	0.8	0.7	11.4	9.2	20.0	3.5	0.9	1.3	34.1	101.0
Southwest (SW)	1.7	4.5	**11.8**	5.8	1.9	0.7	0.5	4.8	5.5	12.0	11.1	4.9	4.6	31.2	101.2
Northwest (NW)	3.4	1.8	2.7	**26.9**	9.4	1.6	0.9	2.9	1.3	2.6	1.9	1.3	13.0	30.8	100.4
West Canada (WC)	1.9	0.6	0.4	5.9	**28.7**	4.8	0.9	2.1	0.3	0.6	0.3	0.3	15.6	37.3	99.8
East Canada (EC)	8.4	3.7	1.2	5.7	17.8	**16.5**	2.9	2.5	0.9	2.2	1.0	0.5	6.7	29.6	99.6
Northeast (NE)	11.8	13.9	2.2	5.6	4.5	3.1	**7.8**	9.6	3.5	9.1	2.3	0.8	3.1	23.0	100.4
Mexico (MX)	0.3	1.3	0.4	0.6	0.3	0.5	0.1	4.3	9.5	12.4	**16.9**	8.4	1.0	43.3	99.3

to August. Also, there is more variability in August than in June and July for SE sources from GM and SE.

Eighteen months of data are used to compute correlations between some of the regional hydrological data. If we assume that the actual number of degrees of freedom is about 15 (allowing for a small month-to-month correlation), a simple statistical significance test based on Fisher's *z* transform (e.g., Stuart and Ord 1994) indicates that correlations with magnitudes greater than 0.5 are significantly different from 0 at the 5% level. If we assume only 12 degrees of freedom, the value must be larger than about 0.6 to be significant. Figure 10 shows the correlations between the local source precipitation (precipitation that originated as evaporation within the region of interest) and region-averaged total precipitation and evaporation. In general, the land regions are characterized by a positive correlation between local precipitation and total precipitation. Barnston and Schikedanz (1984) found that irrigation helped to enhance precipitation only when a mechanism existed to trigger the precipitation. The positive correlation between precipitation and local precipitation may follow that idea, in that local precipitation is large when total precipitation is large. The correlation with evaporation is weaker in some regions. This result is likely because strong evaporation can occur in circumstances in which precipitation cannot occur (such as a significant high pressure center), in which case, local water would diverge from the region.

The SW region has a recycling ratio comparable to those of SE and MW, but the total precipitation is much smaller (Table 2). The SW recycling ratio (Fig. 9) decreases during the course of the summer while there is an increase of the oceanic sources (GM, AT, and TA in Fig. 1). The decrease of SW recycling is related to the seasonal decrease of evaporation (1.30, 0.75, and 0.64 mm day^{-1} for June, July, and August, respectively). This relation is reinforced by a strong correlation between evaporation and recycled precipitation in SW (Fig. 10). The MX region exhibits a decrease of the recycling ratio during the summer while the influence of the BO region increases. This region is known to be strongly impacted by model deficiencies associated with tropical deficiencies. Although the sources should be described better by WVTs incorporated into a reanalysis system, these also can be unreliable. For example, Barlow et al. (1998) find that European Centre for Medium-Range Weather Forecasts reanalysis shows southerly transport for the Mexican-region precipitation, whereas NCEP reanalysis shows easterly flow.

To understand better the relationships among the different source regions, Table 3 shows correlations between the various regions of the amount of precipitation they contribute to the MW and SE regions. These are computed from the monthly mean WVT precipitation (as in Fig. 9). Positive values indicate that certain regions are related to each other, likely through the mean circulation. For example, in the MW region, the source from the Gulf of Mexico is related to the sources in the Atlantic and the tropical Atlantic. In contrast, the sources from the Gulf of Mexico and Eastern Pacific show little correlation. The local source in both the MW and SE regions tends to be more correlated with nearby continental regions' sources than with oceanic sources.

This information can be used to help to understand the relevance of the regions and where additional regions may be needed. In both the MW and SE regions, the Gulf of Mexico is an important source of water and is positively correlated to the sources from the tropical Atlantic and Atlantic regions. Because the Atlantic sources are farther away and, hence, smaller in magnitude, it may be convenient for some studies to combine all the regions together. It is also useful to correlate the different source regions to the complement source to identify other regions with important sources. In these experiments, the complement source in MW is correlated with the Gulf of Mexico, tropical Atlantic, and Atlantic regions (Table 3). This indicates that we should consider the rest of the tropical Atlantic (between the Caribbean and Africa) as a regional tracer to help to explain more of the regional sources of water for the central United States (the SE correlations are somewhat weaker). In MW, the EP regional source is also correlated with the complement, indicating that the greater Pacific Ocean may need to be considered. Likewise, in the SE region, MX and BO are correlated to the com-

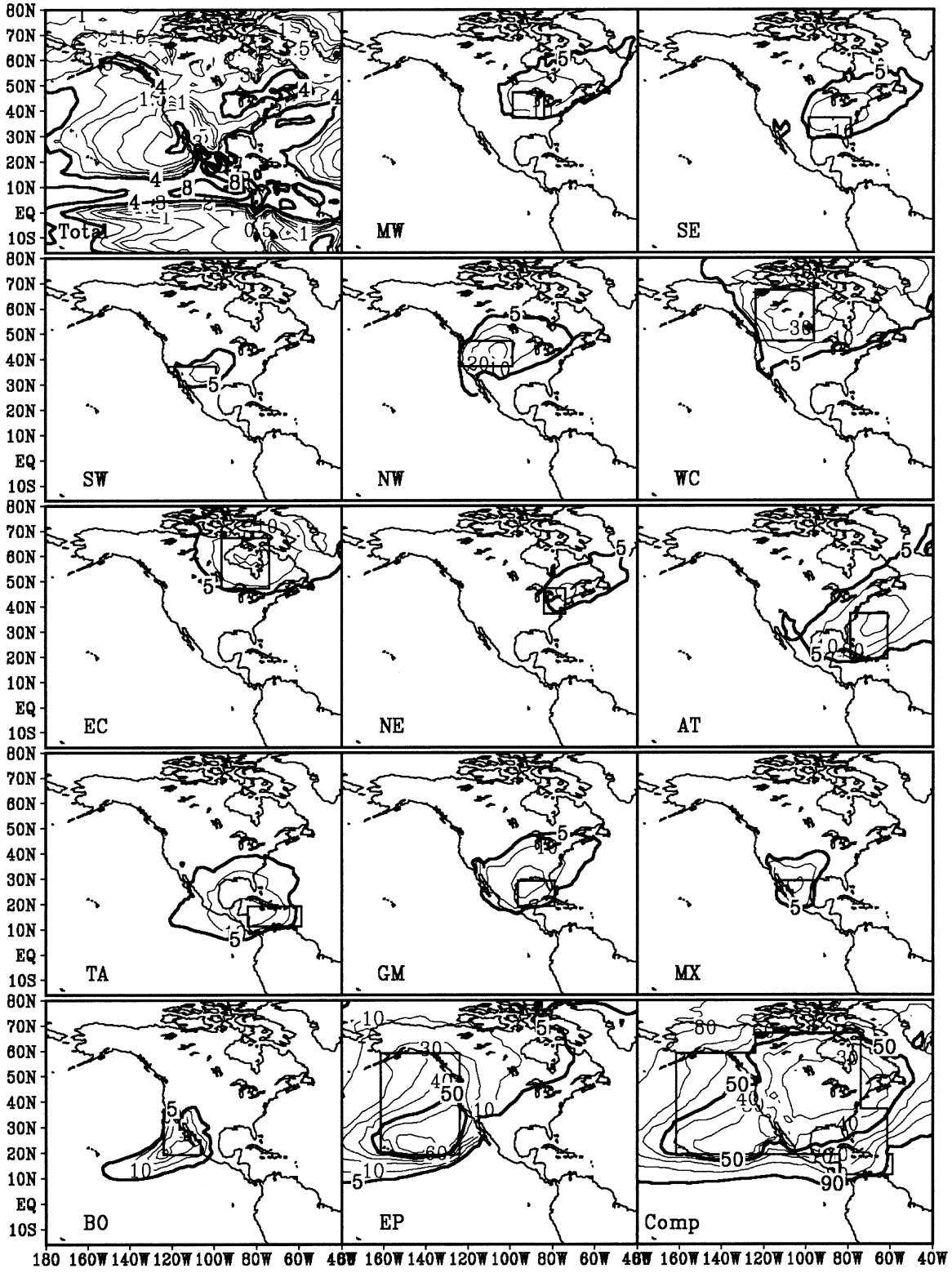

FIG. 7. Total precipitation (mm day^{-1}) for the 6-yr JJA average along with the WVT percentage of the total precipitation for each regional WVT and the complement. The abbreviated name and geographic source region are included in each figure. Precipitation contour intervals are boldface for 0.1, 4, 8, and 16 mm day^{-1}; the light contours are 0.5, 1, 1.5, 2, and 3 mm day^{-1}. WVT contours are every 10% with boldface contours at 5%, 50%, and 90%.

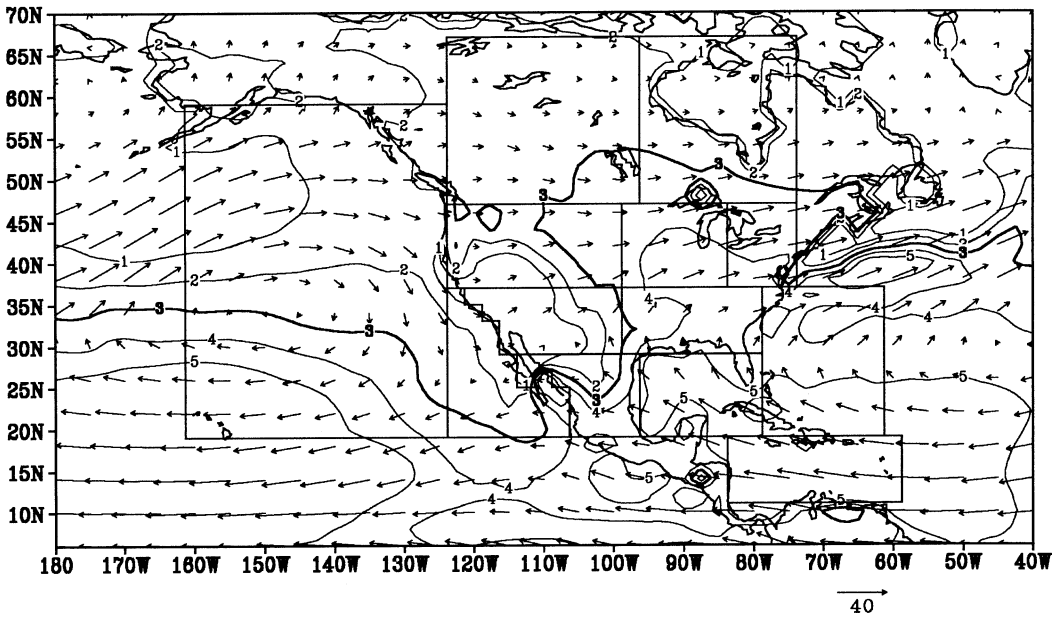

FIG. 8. JJA average water vapor transport [(m s^{-1}) (g kg^{-1}); vector scale is shown and every other gridpoint vector is shown] and evaporation (mm day^{-1}; contoured with values greater than 4 mm day^{-1} shaded).

plement and may indicate that the tropical Pacific Ocean may play a role.

d. Indian local and remote sources of water

The Indian WVTs were computed using the same model constituent tracer arrays as those used for the North American region. The reason for doing this was to test the use of multiple regions in a single tracer to maximize the computational resources and exploit the global model in a regional study. Figure 11 shows the global map of WVT precipitation percentage from the Indian regional tracers along with the companion North American tracers. In general, there is little overlap between the WVTs from the two regions. The most notable exception is the constituent tracer for the AT and northern continental (NC) regions. Precipitation from AT extends very far to the east across Europe, very close to precipitation from NC. However, there is little contribution from AT to IN. In addition, precipitation from the southern Indian Ocean [south oceanic (SO)] region extends westward across the Tropics into South America. Although this likely does not interfere with the EC recycling ratio, it may affect the fraction of precipitation associated with EC in MX (Table 1). The percentage of EC precipitation in MX is 0.51%, slightly greater than that of WC (0.34%) and of SW (0.14%). These contributions are small and do not adversely influence the analysis discussed in the previous section. Nonetheless, if precision is required, multiple regions contributing to a single constituent tracer should not be implemented. However, the overlap of WVT precipitation does not appear overly influential on the regional analysis, so such a multiple-region tracer approach may be useful in some experiments. The amount of precipitation that occurs in the IN region from all of the North American region single tracers (MW, SE, TA, GM, MX, BO, EP) is 0.22% of the total precipitation.

The southern Indian Ocean is one of the most influential WVT regions. Its precipitation is noticeable from

TABLE 2. North American continental regions' JJA precipitation P, evaporation E, recycled precipitation P_T, percentage of recycled precipitation, percentage of recycled evaporation, and area of the region. Note that here percentages do not equal the ratios of seasonal averages, because the percentages are computed from the average of monthly ratios, not from the ratio of seasonal averages.

	P (mm day^{-1})	E (mm day^{-1})	P_T (mm day^{-1})	% of P	% of E	Area (km^2)
MW	4.31	4.03	0.61	14.26	15.12	1.38×10^6
SE	3.37	4.03	0.39	12.72	9.76	1.66×10^6
SW	0.59	0.90	0.08	11.81	7.55	1.60×10^6
NW	1.77	2.39	0.47	26.89	19.48	2.29×10^6
WC	2.62	2.63	0.75	28.71	28.47	3.69×10^6
EC	2.53	1.69	0.41	16.50	24.29	3.02×10^6
NE	3.68	3.81	0.28	7.83	7.50	9.20×10^5
MX	4.66	3.10	0.77	16.94	24.90	1.40×10^6

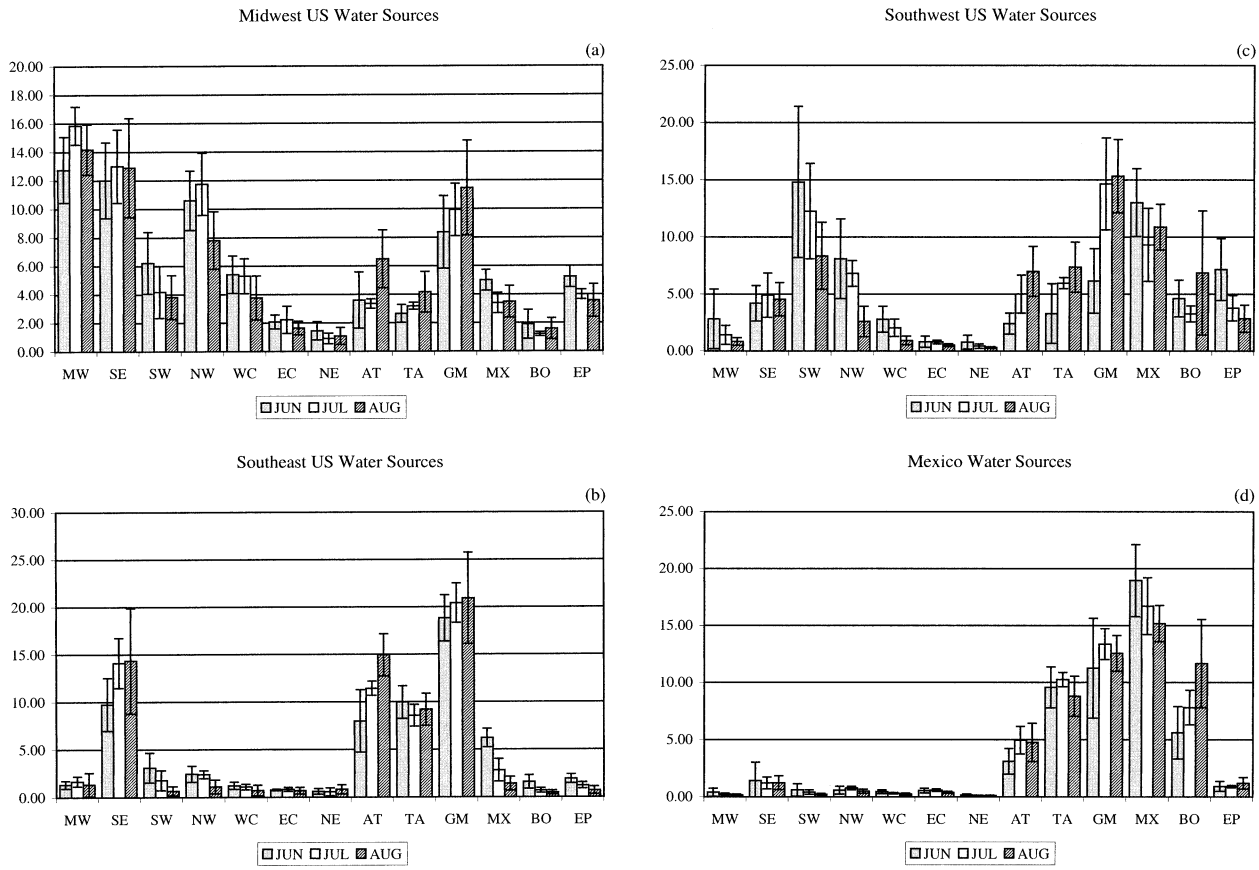

FIG. 9. Percent contribution of evaporation from the North American regions to precipitation in (a) MW, (b) SE, (c) SW, and (d) MX. The bars indicate the monthly means for Jun, Jul, and Aug averaged for all six years, and the error bars indicate one standard deviation of the mean.

40°S to 40°N and across the Tropics to the coast of South America (Fig. 11). Druyan and Koster (1989) found that the Indian Ocean did not contribute to the Sahelian precipitation. However, that study considered a region similar to the western Indian Ocean [west oceanic (WO)] region, which is dominated by low-level monsoon westerly flow. These results indicate that the SO source, which is characterized by low-level easterlies, could impact the Sahelian precipitation.

Water evaporated from the NC region reaches farther east than the southeast Asian coast and nearly to the Aleutian Islands. The other Indian regional WVTs are much more local. Figure 12 shows the seasonal contributions of the Indian regional WVTs to IN precipitation. The regional WVTs account for 85% of the Indian continental precipitation. The recycling ratios in IN are generally smaller than those in the North American region, but the magnitude of recycled precipitation is larger (due to the larger total precipitation). As a result of the low-level monsoon winds and the oceanic evaporation, WO and SO account for about two-thirds of the water that precipitates over India. The WO sources decrease throughout the summer while the SO sources increase. The variability of the SO and WO sources is small when compared with the variability of the important oceanic sources in North America.

e. Bulk diagnostic recycling

To quantify precipitation recycling, Brubaker et al. (1993) and Eltahir and Bras (1994) developed diagnostic

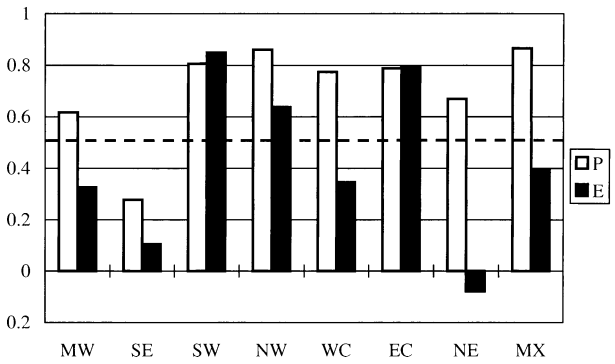

FIG. 10. Correlation coefficients of all the North American continental regions' local precipitation (recycled precipitation) with total precipitation and evaporation. Computed from monthly means of six JJAs. The dashed line indicates 0.5 correlation.

TABLE 3. Correlation coefficients of all the sources of water for the MW region (top) and the SE region (bottom) precipitation (computed from 18 monthly mean values). Positive correlations greater than 0.5 are boldface. Rows and columns are sorted by the mean percentage of precipitation from each region so that the largest sources are down to the right.

MW region	NE	BO	EC	TA	MX	EP	AT	SW	WC	GM	NW	SE	MW
NE	1.00												
BO	0.28	1.00											
EC	**0.65**	0.18	1.00										
TA	0.07	−0.47	0.05	1.00									
MX	0.43	0.40	0.37	0.24	1.00								
EP	**0.65**	0.30	**0.55**	−0.12	**0.63**	1.00							
AT	0.11	−0.24	−0.06	0.47	0.14	−0.07	1.00						
SW	0.25	0.13	0.31	0.00	**0.79**	**0.65**	0.10	1.00					
WC	0.48	0.09	**0.61**	−0.12	0.37	**0.82**	−0.04	**0.58**	1.00				
GM	0.17	−0.25	0.24	**0.84**	0.42	0.07	**0.57**	0.14	−0.03	1.00			
NW	0.19	0.15	0.50	−0.04	**0.56**	**0.65**	−0.29	**0.64**	**0.71**	0.01	1.00		
SE	0.17	0.14	0.23	0.08	0.38	**0.55**	0.27	0.37	**0.52**	0.33	0.42	1.00	
MW	0.41	0.21	**0.73**	0.09	0.27	0.48	−0.31	0.13	**0.52**	0.21	**0.67**	0.33	1.00
Comp	0.48	0.29	0.44	**0.54**	**0.77**	**0.53**	0.22	0.42	0.31	**0.69**	0.43	0.40	0.45

SE region	NE	EC	WC	BO	MW	EP	SW	NW	MX	TA	AT	SE	GM
NE	1.00												
EC	0.24	1.00											
WC	0.31	**0.71**	1.00										
BO	0.10	**0.71**	**0.62**	1.00									
MW	0.09	0.49	**0.71**	0.28	1.00								
EP	0.27	**0.75**	**0.91**	**0.76**	**0.61**	1.00							
SW	0.17	**0.55**	**0.70**	**0.55**	0.39	**0.78**	1.00						
NW	0.09	**0.63**	**0.85**	**0.57**	**0.83**	**0.85**	**0.71**	1.00					
MX	0.11	**0.79**	**0.71**	**0.91**	0.34	**0.84**	**0.79**	**0.65**	1.00				
TA	0.08	**0.61**	0.41	**0.51**	0.13	**0.57**	0.43	0.38	**0.60**	1.00			
AT	−0.12	0.03	−0.27	−0.15	−0.33	−0.25	−0.31	−0.33	−0.17	0.50	1.00		
SE	−0.09	0.29	0.18	−0.02	0.41	0.10	−0.03	0.39	−0.01	0.22	0.16	1.00	
GM	−0.22	0.49	0.16	0.49	−0.08	0.32	0.21	0.18	**0.51**	**0.86**	**0.61**	0.32	1.00
Comp	0.03	**0.61**	0.32	**0.59**	0.11	0.49	0.32	0.33	**0.59**	**0.93**	**0.53**	0.16	**0.85**

routines, based on the water balance, to compute precipitation recycling from monthly mean gridded fields (precipitation, evaporation, and vertically integrated moisture transport). The bulk diagnostic recycling ratios for the MW and SE regions have been computed using these methods (as in Bosilovich and Schubert 2001). The difference between these bulk diagnostic methods and the WVT recycling is that the WVT local precipitation is computed at each model time step using the model's physical tendencies. The WVT precipitation recycling can be considered as a quantitative estimate within the uncertainty discussed earlier and within the context of the GCM simulation. Therefore, the WVT precipitation recycling can be used to validate the simpler bulk diagnostic estimates of precipitation recycling.

Figure 13 shows the MW and SE recycling ratios for each month of the simulation from each method. In the MW region, the WVT recycling ratio is generally between the larger values of Eltahir and Bras (1994) and the lower values of Brubaker et al. (1993). Savenije (1995), Dirmeyer and Brubaker (1999), and Bosilovich and Schubert (2001) all find that the Brubaker method underestimates the precipitation recycling. This is apparent for the MW region; in the SE region, however, the WVT recycling ratio is less than the values of both bulk diagnostic methods. The implication is that water evaporated within the SE region is more likely to leave the region than is suggested by either bulk diagnostic method. Savenije (1995) attributes the systematic differences of the Brubaker bulk method to using monthly area-averaged hydrologic data. This may be appropriate for the MW region but does not hold for the SE region.

Table 4 shows the correlations of the MW and SE regions' monthly mean hydrologic data (precipitation and evaporation) with the bulk diagnostic recycling estimates (recycled precipitation) in addition to the WVT local source of precipitation. In the MW region, all the local precipitation methods are positively correlated with total precipitation. However, the SE WVT local precipitation is weakly correlated to total precipitation, and the bulk methods are even less correlated. Despite these differences, the recycled precipitation from each method is positively correlated in both the MW and SE regions (although the SE bulk method correlations with WVT are weak). Trenberth (1999) suggested that the bulk methods of precipitation recycling be considered as an index of precipitation recycling rather than as a quantitative estimate. The large biases of the bulk diagnostic methods (Fig. 13) and the positive correlation with WVT recycling (Table 4) indeed indicate that the bulk diagnostic data could be used internally as indicators of recycling. Again, the evaporation shows little

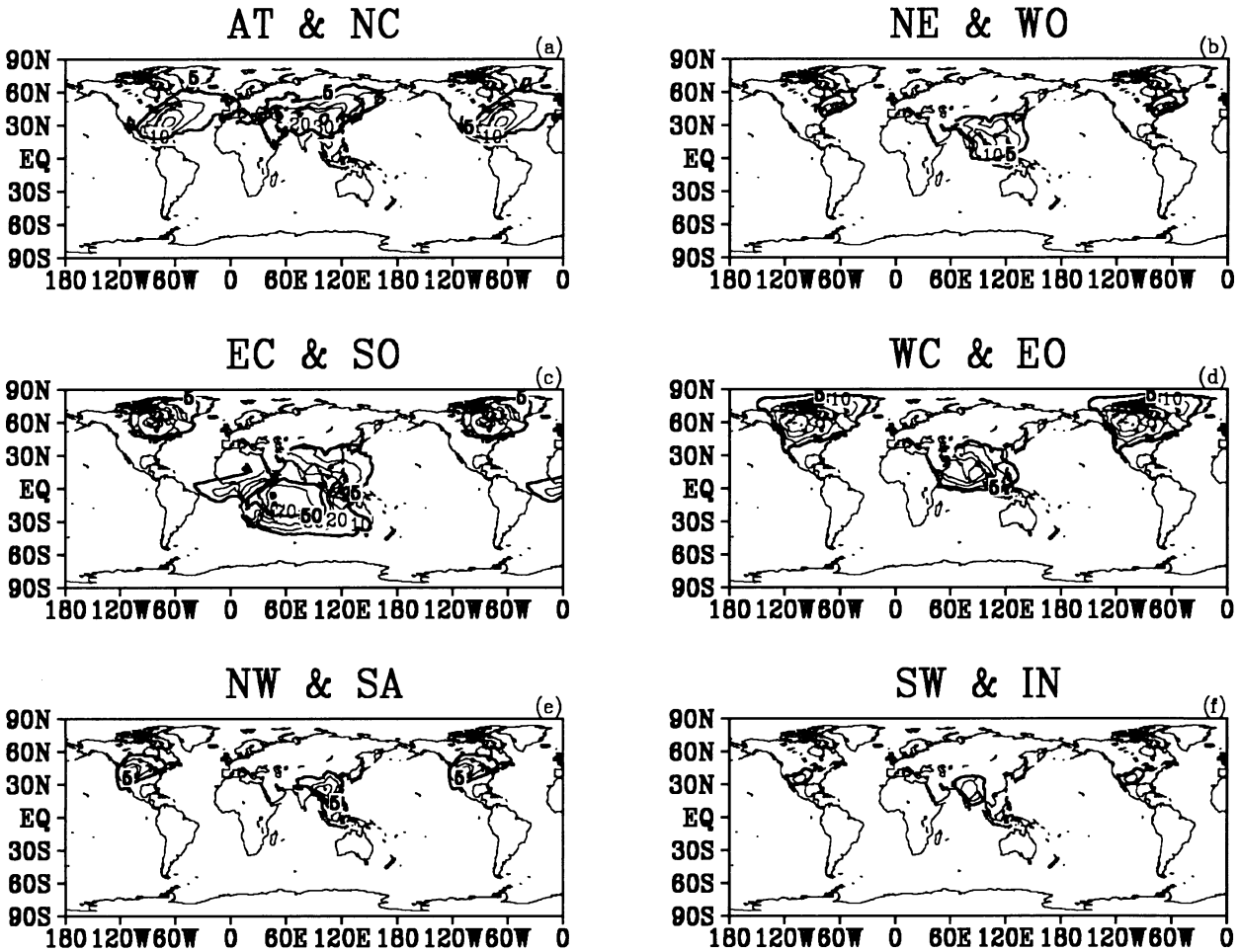

FIG. 11. Percent of precipitation for the 6-yr JJA average of the IN regional WVTs. WVT contours are every 10%, with boldface contours at 5%, 50%, and 90%. These WVTs overlap with North American WVTs, and a global map is provided to examine the potential for interference of one region with another.

or no correlation with the bulk-method local precipitation. One interpretation is that the largest evaporation events do not necessarily provide large local sources of precipitation.

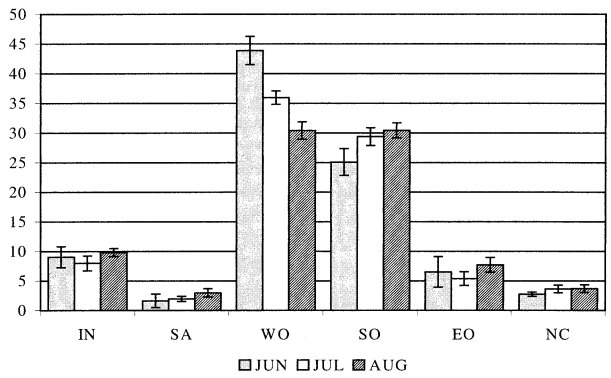

FIG. 12. Percent contribution of Indian regional evaporative sources to IN precipitation.

4. Summary and discussion

To compute the local and remote sources of water for regional precipitation, water vapor tracers have been implemented into the NASA GEOS GCM, following coarse-resolution experiments by Koster et al. (1986) and Joussaume et al. (1986). Six summer seasons were simulated with regional tracers designed to explain better the local and remote sources of water for the central United States and the Indian continental precipitation. The purpose of this experiment is to demonstrate the methodology, the validation, and the analysis of the water vapor tracer methodology applied to regional hydrologic cycles. Model physics affects the specific values of local and remote precipitation, and the physics will vary from model to model. A more rigorous validation of the WVT methodology (as compared with previous studies) indicates that our initial implementation of the tracers emulates the model's time- and area-averaged precipitation and water vapor with acceptably small differences from GCM calculations (typically

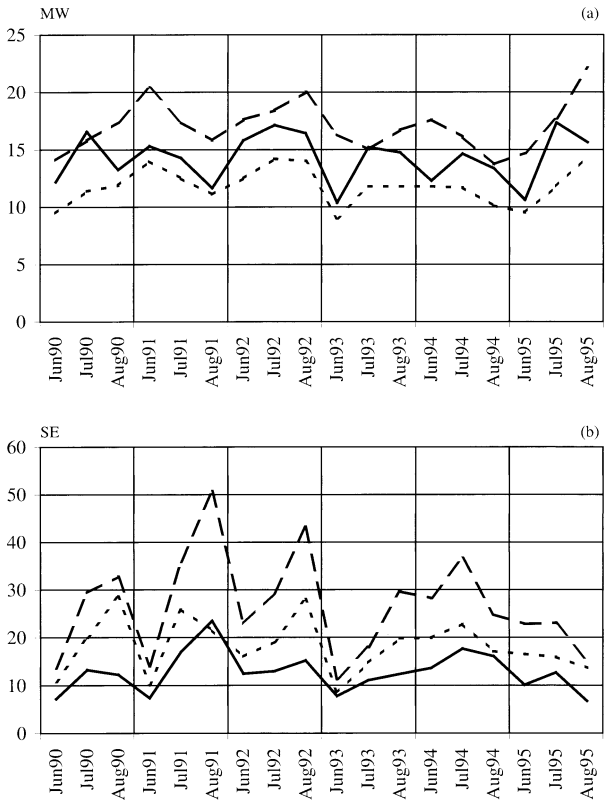

FIG. 13. Percentage of precipitation recycling for each simulated month for the WVTs (solid), Eltahir and Bras (1994; long dash), and Brubaker et al. (1993; short dash) in the (a) MW and (b) SE regions.

TABLE 4. Correlation coefficients (computed from monthly means of six JJAs) of precipitation P, evaporation E, Eltahir and Bras (1994) local precipitation P_E, Brubaker et al. (1993) local precipitaion P_B, and WVT local precipitation P_T for MW and SE.

	P	E	P_T	P_E	P_B
MW					
P	1.00				
E	−0.27	1.00			
P_T	0.62	0.33	1.00		
P_E	0.80	−0.18	0.72	1.00	
P_B	0.66	0.17	0.88	0.87	1.00
SE					
P	1.00				
E	0.22	1.00			
P_T	0.28	0.10	1.00		
P_E	−0.08	−0.12	0.54	1.00	
P_B	0.18	0.01	0.46	0.87	1.00

within 1% of the model's predicted monthly precipitation).

The results of the analysis of the tracer diagnostics for this simulation are as follows.

1) More than 50% of the precipitation in the midwestern United States came from continental regional tracers, and the local source was the largest of the regional tracers (at 14%).
2) Eighteen percent of midwestern precipitation came from the Gulf of Mexico and Atlantic Ocean tracers.
3) Statistical correlations suggest that a portion of the complement tracer is related to the Gulf of Mexico and tropical Atlantic sources, so that extending the regional tracers farther east toward Africa may explain more of the central U.S. precipitation.
4) In general, most North American land regions showed a positive correlation between recycled precipitation and total precipitation. This is analogous to previous results that show that local sources of water can increase precipitation only if there exists a mechanism for precipitation (Barnston and Schikedanz 1984).
5) The correlation of the local precipitation with evaporation was not as strong in some regions. This result likely is related to strong evaporative events that may occur when precipitation cannot (e.g., wet surface and a dominant high pressure circulation).
6) Local precipitation in MW and SE is more correlated with nearby continental sources of water than with oceanic sources (though the signal is weaker in SE).
7) The bulk diagnostic methods of precipitation recycling had some large biases in comparison with WVT recycling. However, the correlations of the bulk diagnostic cases tested here were positive with WVT recycling, indicating that the bulk methods may provide a useful index of recycling.
8) Using one tracer array to simulate more than one regional source of water did not overly influence any of the results. However, it can be distracting and may not be desirable for all purposes.
9) The western Indian Ocean provides the largest source of water vapor over continental India. This source is largest in June and decreases through August. The southern Indian Ocean provides a significant source of water for India and also for the Sahel.

These diagnostic tracers provide additional quantitative information on the regional hydrologic cycle. Such diagnostics would be useful in sensitivity simulations. For example, testing the sensitivity to soil water initialization leads to different local and remote sources of precipitation for wet and dry cases. Without additional diagnostic data, it is impossible to quantify the difference in local and remote sources of water from the difference in precipitation caused by thermodynamic perturbations (Bosilovich and Sun 1999a,b).

The complement tracer served its purpose for the validation exercise, but it would be much more useful if the complement was broken up into several continental-scale water vapor tracers. In this way, continental and oceanic sources of water for any region could be determined. In addition, the correlation statistics may be served better through correlation with continental-scale tracers. The primary deficiency of the WVT method-

ology is that if the WVTs are not defined properly at the beginning of experimentation then the simulation will need to be redone. For example, the midwestern U.S. precipitation may be defined better by a more rigorous tracking of the tropical Atlantic evaporative sources, and Mexican regional hydrological behavior requires a more careful consideration of the tropical sources of water. This is not an issue with diagnostic approaches (as in Dirmeyer and Brubaker 1999). Furthermore, the results from a GCM simulation are also limited by the GCM's ability to simulate the physical processes, climate circulation, and variability. However, the data can provide additional quantitative analysis of the regional hydrological behavior with regard to climate variations and extremes, within the context of the global model. Applications within a global data assimilation system will provide better estimates of the local and remote sources of water in real-data case studies.

Acknowledgments. Drs. Yogesh Sud, Robert Atlas, and Paul Dirmeyer have provided many useful discussions on this research. Suggestions from the anonymous reviewers greatly improved the final manuscript. The development of the code was completed with assistance from Greg Walker, Andrea Molod, and Larry Takacs. This research was partially funded by the Joint GCIP/PACS Warm-Season Precipitation Initiative.

REFERENCES

Barlow, M., S. Nigam, and E. H. Berbery, 1998: Evolution of the North American monsoon system. *J. Climate,* **11,** 2238–2257.

Barnston, A. G., and P. T. Schikedanz, 1984: The effect of irrigation on warm season precipitation in the southern Great Plains. *J. Climate Appl. Meteor.,* **23,** 865–888.

Bosilovich, M. G., and W.-Y. Sun, 1999a: Numerical simulation of the 1993 Midwestern flood: Land–atmosphere interactions. *J. Climate,* **12,** 1490–1505.

——, and ——, 1999b: Numerical simulation of the 1993 Midwestern flood: Local and remote sources of water. *J. Geophys. Res.,* **104D,** 19 415–19 424.

——, and S. D. Schubert, 2001: Precipitation recycling in the GEOS-1 data assimilation system over the central United States. *J. Hydrometeor.,* **2,** 26–35.

Brubaker, K. L., D. Entekahabi, and P. S. Eagleson, 1993: Estimation of precipitation recycling. *J. Climate,* **6,** 1077–1089.

Chou, M. D., 1984: Broadband water vapor transmission functions for atmospheric IR flux computations. *J. Atmos. Sci.,* **41,** 1775–1778.

Dirmeyer, P. A., and K. L. Brubaker, 1999: Contrasting evaporative moisture sources during the drought of 1988 and the flood of 1993. *J. Geophys. Res.,* **104,** 19 383–19 398.

Druyan, L. M., and R. D. Koster, 1989: Sources of Sahel precipitation for simulated drought and rainy seasons. *J. Climate,* **2,** 1438–1446.

Eltahir, E. A. B., and R. L. Bras, 1994: Precipitation recycling in the Amazon basin. *Quart. J. Roy. Meteor. Soc.,* **120,** 861–880.

——, and ——, 1996: Precipitation recycling. *Rev. Geophys.,* **34,** 367–378.

Harshvardhan, R. Davies, D. A. Randall, and T. G. Corsetti, 1987: A fast radiation parameterization for atmospheric circulation models. *J. Geophys. Res.,* **92,** 1009–1016.

Helfand, H. M., and J. C. Labraga, 1988: Design of a nonsingular level 2.5 second-order closure model for prediction of atmospheric turbulence. *J. Atmos. Sci.,* **45,** 113–132.

——, and S. D. Schubert, 1995: Climatology of the simulated Great Plains low-level jet and its contribution to the continental moisture budget of the United States. *J. Climate,* **8,** 784–806.

——, A. Molod, and M. G. Bosilovich, 1999: Implications of a moist turbulence parameterization for the numerical prediction of the structure and properties of the atmospheric boundary layer. Preprints, *13th Conf. on Numerical Weather Prediction,* Denver, CO, Amer. Meteor. Soc., 54–59.

Higgins, R. W., Y. Yao, E. S. Yarosh, J. E. Janowiak, and K. C. Mo, 1997: Influence of the Great Plains low-level jet on summertime precipitation and moisture transport over the central United States. *J. Climate,* **10,** 481–507.

Huang, J., H. M. van den Dool, and K. P. Georgakakos, 1996: Analysis of model-calculated soil moisture over the United States (1931–1993) and applications to long-range temperature forecasts. *J. Climate,* **9,** 1350–1362.

Joussaume, S., R. Sadourny, and C. Vignal, 1986: Origin of precipitating water in a numerical simulation of July climate. *Ocean–Air Interact.,* **1,** 43–56.

Klein, W. H., and H. J. Bloom, 1989: An operational system for specifying monthly precipitation amounts over the United States from the field of concurrent mean 700-mb heights. *Wea. Forecasting,* **4,** 51–60.

Koster, R. D., and M. J. Suarez, 1992: Modeling the land surface boundary in climate models as a composite of independent vegetation stands. *J. Geophys. Res.,* **97,** 2697–2715.

——, J. Jouzel, R. Suozzo, G. Russell, W. Broecker, D. Rind, and P. Eagleson, 1986: Global sources of local precipitation as determined by the NASA/GISS GCM. *Geophys. Res. Lett.,* **13,** 121–124.

Lin, S.-J., and R. B. Rood, 1996: Multidimensional flux-form semi-Lagrangian transport schemes. *Mon. Wea. Rev.,* **124,** 2046–2070.

Moorthi, S., and M. J. Suarez, 1992: Relaxed Arakawa–Schubert: A parameterization of moist convection for general circulation models. *Mon. Wea. Rev.,* **120,** 978–1002.

Numagati, A., 1999: Origin and recycling processes of precipitating water over the Eurasian continent: Experiments using an atmospheric general circulation model. *J. Geophys. Res.,* **104,** 1957–1972.

Peixoto, J. P., and A. H. Oort, 1992: *Physics of Climate.* American Institute of Physics, 520 pp.

Reynolds, R. W., and T. M. Smith, 1994: Improved global sea surface temperature analyses using optimum interpolation. *J. Climate,* **7,** 929–948.

Savenije, H. H. G., 1995: New definitions for moisture recycling and the relation with land use change in the Sahel. *J. Hydrol.,* **167,** 57–78.

Simpson, J. J., J. S. Berg, C. J. Koblinsky, G. L. Hufford, and B. Beckley, 2001: The NVAP global water vapor data set: Independent cross comparison and multi year variability. *Remote Sens. Environ.,* **76,** 112–129.

Stuart, A., and J. K. Ord, 1994: *Kendall's Advanced Theory of Statistics.* Halsted Press, 676 pp.

Suarez, M. J., and L. L. Takacs, 1995: Documentation of the ARIES/GEOS dynamical core: Version 2. NASA Tech. Memo. 104606, Vol. 5, 58 pp.

Sud, Y. C., and A. Molod, 1988: The roles of dry convection, cloud-radiation feedback processes and the influence of recent improvements in the parameterization of convection in the GLA GCM. *Mon. Wea. Rev.,* **116,** 2366–2387.

Trenberth, K. E., 1999: Atmospheric moisture recycling: Role of advection and local evaporation. *J. Climate,* **12,** 1368–1381.

Xie, P., and P. A. Arkin, 1997: Global precipitation: A 17-year monthly analysis based on gauge observations, satellite estimates, and numerical model outputs. *Bull. Amer. Meteor. Soc.,* **78,** 2539–2558.